11th ANKARA INTERNATIONAL AEROSPACE CONFERENCE AIAC-2021-136
8-10 September 2021 - METU, Ankara TURKEY

SPATIAL RESOLUTION AND MODULATION TRANSFER FUNCTION ANALYSES FOR SATELLITE IMAGING

Kamil B. Alici [1]
The Scientific and Technological Research Council of Turkey,
Space Technologies Research Institute (TUBITAK UZAY), Remote Sensing Group,
Ankara, 06800 Turkey

ABSTRACT

Modulation Transfer Function (MTF) is one of the most important and fundamental image quality metrics. In the present paper, we present results of image chain simulation, spatial resolution, Contrast Transfer Function (CTF), and MTF analyses, obtained by using a multi pattern synthetic ground truth (SGT) image. This synthetic image includes slanted edge patterns with various angles, bar patterns with varying spatial frequencies, horizontal and vertical hyperbolic wedge patterns, sine wave star pattern, and example architectures utilized in National imagery interpretability rating scale (NIIRS) determination. Utilization of this SGT allows quantitative study of correspondence between the spatial resolution and the MTF/CTF values for low earth orbit (LEO) satellite imaging.

INTRODUCTION

Accurate determination of one of the most important image quality metrics, modulation transfer function (MTF), with minimized error margin is of significant importance for satellite imaging studies [1-16]. In literature, a number of standard test patterns have been utilized to determine the MTF metric of camera output images [Alici K., 2017; Alici K., 2017; Alici K., 2018; Alici K., 2019; Alici K., 2020; Alici K., 2021; Blahut R., 2004; Boreman G., 2001; Brigham E., 1988; EMVA, 2010; Fiete R., 2010; Gaskill J., 1978; Holst G, 2011; ISO, 2017; Schott J., 2007; Tzannes A., 1995]. Mostly utilized test target patterns are listed as: bar patterns with various spatial frequencies, sine wave stars, hyperbolic wedges, and slanted edges [Alici K., 2020; Blahut R., 2004; Boreman G., 2001; Brigham E., 1988; Fiete R., 2010; Gaskill J., 1978; Holst G, 2011; ISO, 2017; Schott J., 2007].

There are many experimental studies for the estimation and determination of MTF [Estribeau M., 2004; Estribeau M., 2005; Li T., 2011; Tzannes A., 1995]. The slanted edge response utilizes a sharp, high contrast, slightly tilted edge image gathered by the (satellite) camera system. In this technique, we obtain the edge spread function (ESF) by using oversampling method. Corresponding line spread function (LSF) is obtained by using first order derivation, and finally, MTF is obtained by using Fourier Transform [ISO, 2017; Li T., 2011; Tzannes A., 1995]. A number of fitting and filtering methods also studied to improve this methodology [ISO, 2017; Li T., 2011].

[1] Assoc. Prof. Dr. in a TUBITAK Space Technologies Research Institute, Email: kamil.alici@tubitak.gov.tr

We studied image chain approach to estimate the image quality of spaceborne satellite images [Alici K., 2017; Alici K., 2017; Alici K., 2018; Alici K., 2019; Alici K., 2020; Alici K., 2021]. In our initial endeavors, we used relatively high resolution images obtained by using airborne platforms as input to our simulations. These ground truth (GT) input images have 3-4 times better ground sampling distance (GSD) than the satellite platform of interest. Also these GT images have relatively high signal to noise ratio (SNR) values. Recently, we initiated studies on the generation of synthetic images [Alici K., 2020] that have features in accordance with National imagery interpretability rating scale (NIIRS) values [Ali M., 2016; Cota S., 2009; Harrington L., 2015; Irvine J., 1997; Leachtenauer J., 1997]. We aim to compare and match results of several MTF analysis methods by using these synthetic ground truth (SGT) images [Alici K., 2019; Alici K., 2020].

Utilization of standard target patterns in combination with selected real world architectures allows us to obtain and compare results of a number of different satellite image analysis methodologies. In the present paper, we provide design, image chain simulations, spatial resolution analysis and MTF analysis of an earth observation satellite (AnkaraSat-3) operating at the low earth orbit. Computed satellite overall MTF was used as input for the corresponding contrast transfer function (CTF) calculations. Spatial resolution is determined by using linear search algorithms operated on estimated satellite image patterns such as horizontal hyperbolic zone plate. Resolution values obtained from hyperbolic wedge patterns and computed by using GSD formula are in good agreement for detector limited systems. Further comparative studies that include sine wave star patterns, slanted edge patterns and bar target pattern results will be reported upon completion.

THEORETICAL BACKGROUND

It is possible to estimate image quality of ground based and spaceborne camera systems before they are physically constructed and became operational [Alici K., 2019; Babusiaux C., 2005; Bonier A., 1999; Börner A., 2001; Coppo P., 2013; Cota S., 2011; Farrell J., 2003; Filbee D., 2002; Gilmore M., 1999; Hook R., 2008; Krist J., 2011; Limbach M., 2014; Moorhead I., 2001; Ryan R., 2003; Segl K., 2012; Segl K., 2015]. Below, we briefly explain our end-to-end imaging chain approach and details of our SGT image. Due to computational limitations, this paper utilizes a SGT that includes NIIRS patterns that cover values from 2 to 8. Besides, only optical diffraction, detector aperture and linear motion effects could be considered in the reported simulations. We show here a section of our SGT image (horizontal hyperbolic wedge pattern) in the simulation results figure. We plan to cover all ICS effects by future advancements in our computational facilities with available configurations [Berk A., 1987; Mathworks, 2021; Spectral Sciences Inc., 2021; Thinkmate, 2021].

Image Chain Simulation (ICS) Theory

Spaceborne optical systems composed of large scale telescopes and digital imaging sensors have been utilized as EOS cameras. Image quality metrics of space systems can be estimated even before the spacecraft launch [Alici K., 2019; Chen T., 2003; Rojas F., 2002; Taylor E., 2000; Turner M., 2000]. The end-to-end mathematical models and methods developed throughout this direction include atmospheric effects [Fried D., 1966; Fried D., 1966; Goodman J., 2015; Goody R., 1995; Green R., 1998; Hufnagel R., 1964; Hulst H., 1981; Kovalevsky J., 2013; Lei F., 1993; Majumdar A., 2010; Packard C., 2015; Sadot D., 1994; Salvaggio C., 1994] (turbulence, aerosol), blurring effects based on optics [
O'Neill E., 1956; Welford W., 2017] (optical diffraction, manufacturing and misalignment based optical aberrations), image sensor (composed of solid state detectors and electronic circuits) based effects [Barnard K., 1991; Blahut R., 2004; Boreman G., 2001; Brigham E., 1988; Cox J., 1989; Estribeau M., 2005; Fiete R., 2010; Gaskill J., 1978; Holst G, 2011; Iftekharuddin K., 1993; Li J., 2006; Mendis S., 1994; Mersereau R., 1987; Schott J., 2007; Yadid-Pecht O., 2000] such as pixel size, pixel pitch, pixel cross-talk, mismatch in time delay and integration, satellite platform motion [Boreman G., 2001; Fiete R., 2010; Holst G, 2011; Schott J., 2007] (orbital motion based smear, high frequency jitter based smear, look angle effects, maneuver effects, imperfect control based oscillation effects). Moreover, we

incorporate SGT images that have no noise, high sampling rate, and include scaled standard resolution target patterns and planar real world architectures such as roads, railways, wagons, cars, car window wipers [Alici K., 2020; Leachtenauer J., 1997]. Our SGT images are going to be improved by incorporating exact sun radiance calculations [Holst G, 2011; Schott J., 2007], surface reflectance (BRDF) properties [Elson J., 1983; Harvey J., 2012] and three-dimensional rendering algorithms [Schott J., 2007; Schott J., 2012].

ICS aims to cover complete radiometric and spatial analyses and provides mission specific satellite image estimates and related image quality metrics such as SNR, MTF, GSD, MTFA, and GIQE [Alici K., 2019; Leachtenauer J., 1997; Schott J., 2007]. In the present paper, we investigate the satellite image quality by using ICS approach that includes optical diffraction, pixel/detector aperture, and linear motion effects. Fundamental theoretical formalism for these effects is provided below. We set the satellite motion direction as *y-axis* (Along Track, ALT), the line scan type imaging sensors are positioned in parallel to the *x-axis* (Across Track, ACT) and the axis perpendicular to earth surface is selected as z-axis. Our satellite camera points in *−z-direction* and looks perpendicular to the earth (nadir view).

Optical Diffraction, Pixel Aperture, and Linear Motion Smear

We compute the point spread function due to optical diffraction by using the following formula [Alici K., 2017; Alici K., 2019; Brigham E., 1988; Gaskill J., 1978; Schott J., 2007]:

$$PSF(x,y) = \frac{|\mathrm{FT}\{\mathrm{p(x,y)}\}|^2}{(\lambda f)^2 \int \int_{-\infty}^{\infty} \mathrm{p(x,y)dxdy}} \tag{1}$$

In this equation, $p(x,y)$ is the pupil function, $FT\{p(x,y)\}$ represents the two-dimensional Fourier Transform of the pupil function calculated at $f_x = x/\lambda f$, $f_y = y/\lambda f$ spatial frequencies. λ is the operation wavelength, and f is the effective focal length of the satellite telescope.

Pixel aperture MTF depends on the photosensitive area geometry [Barnard K., 1991; Boreman G., 2001; Cox J., 1989; Estribeau M., 2005; Iftekharuddin K., 1993; Li J., 2006; Mendis S., 1994; Mersereau R., 1987; Yadid-Pecht O., 2000], and for rectangular apertures it is calculated by the following formula [Alici K., 2019; Boreman G., 2001; Fiete R., 2010; Holst G, 2011]:

$$MTF_p = \frac{|\sin(\pi\, \mathrm{d_x}\, \mathrm{f_x})\, \sin(\pi\, \mathrm{d_y}\, \mathrm{f_y})|}{\mathrm{d_x}\, \mathrm{d_y}\, \mathrm{f_x}\, \mathrm{f_y}\, \pi^2} \tag{2}$$

Here, d_x and d_y are the physical lengths of the photosensitive areas in each direction.

Linear motion blurs the image as the total signal is integrated along the motion direction during exposure time [Alici K., 2019; Boreman G., 2001; Fiete R., 2010; Holst G, 2011]. Linear motion during exposure time blurs the image as the total signal is integrated along the motion direction. Corresponding MTF is calculated as follows [Alici K., 2019; Boreman G., 2001; Fiete R., 2010; Holst G, 2011]:

$$MTF_s = \frac{|\sin(\pi\, \mathrm{d_y smear}\, \mathrm{f_y})|}{\mathrm{d_y smear}\, \mathrm{f_y}\, \pi} \tag{3}$$

Here, *$d_y$smear* is the length of the smear in the *y-direction* (Along-Track, ALT).

Synthetic Ground Truth (SGT) Image

We have generated a SGT that includes a number of test patterns as shown in Figure 1 in portrait orientation. From left to right, the first pattern is slanted edge with tilt angle 5° for across track (ACT) MTF computation. Below this pattern, we positioned slanted edge with 5°tilt angle that is used for along track (ALT) MTF computation. In the left most third row, we have another slanted edge that is used to compute ACT MTF and it has 10°tilt angle. The next pattern is the vertically aligned hyperbolic wedge, which provides system resolution from contrast studies. Next to the vertical hyperbolic wedge, we placed the sine wave star pattern, also known as the Siemens star. This pattern includes varying spatial frequency components and can be used to determine MTF values. Following patterns are used to imitate real world architectures and implemented by using broadly available data of US standards. We have highway roads, sedan and station cars with windows and wipers, railways, two types of

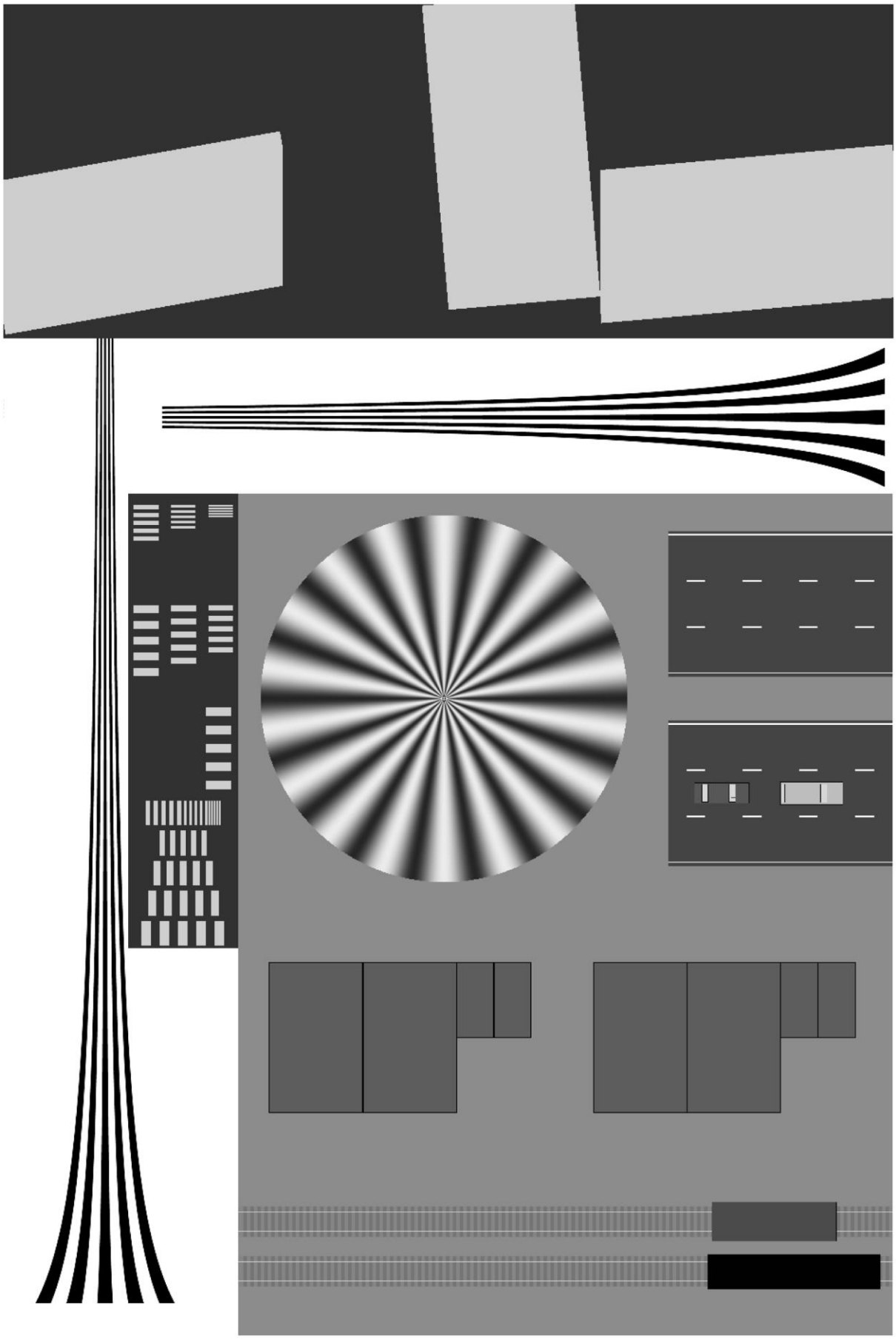

Figure 1: Synthetic Ground Truth (SGT) Image with 3.5cm pixel size.

wagons, and a number of houses. At the right bottom, we placed several bar targets with varying spatial frequencies and a horizontal hyperbolic wedge pattern.

The size of this SGT could be increased in the lateral direction to cover a number of other patterns specific for the study of interest. However, computer memory limitations come into play as the size of the SGT increase. In the present study, we were able to utilize this SGT by dividing it into image patches and using image stitching techniques after each ICS simulation.

RESULTS AND DISCUSSION

Image Chain Simulation: Optical Diffraction, Detector Aperture, and Smear Effects

In this subsection, we present ICS results that incorporate optical diffraction, pixel detector aperture (detector footprint) and linear motion effects. Most parameters of our hypothetical satellite, named as AnkaraSat-3, were given in our previous papers [Alici K., 2017; Alici K., 2018; Alici K., 2019; Alici K., 2020]. The satellite operates at a polar orbit with 567 km altitude and aims to pass over a specific location in Ankara, TURKEY as much as possible. MATLAB computation of spectral radiance from earth surface with assumed 0.2 uniform albedo and 23% atmospheric absorption coefficient and corresponding MODTRAN Ground Reflect (GR) result at the top of the atmosphere (TOA) are given in Figure 2 [Berk A., 1987; Mathworks, 2021; Spectral Sciences Inc., 2021]. The optical aperture of the satellite telescope is 0.70 m and it is assumed to operate at diffraction limited performance (none of the optical aberrations included in the simulations). The imaging sensor pixels and photosensitive area has rectangular geometry with pixel pitch equal to 5.88 *μm*, that corresponds to 85.0 L/*mm*

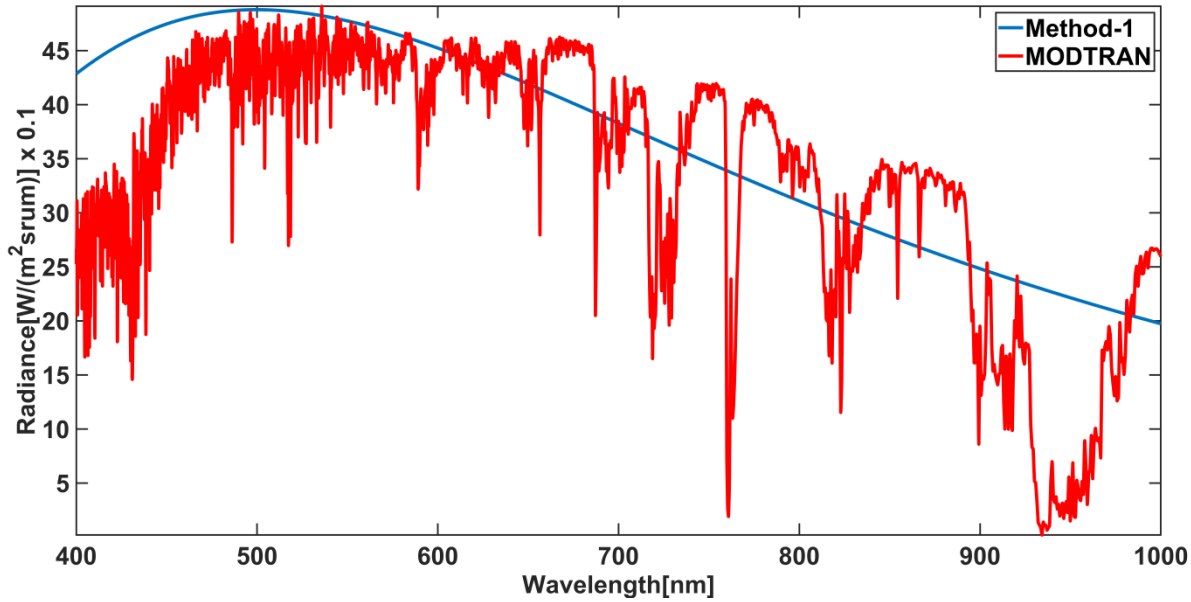

Figure 2: Spectral Radiance from earth surface with assumed 0.2 uniform albedo and 23% atmospheric absorption coefficient and corresponding MODTRAN Ground Reflect (GR) result at the top of the atmosphere (TOA).

Nyquist Frequency (NF). In Figure 3(a), we show the system MTF (optical diffraction + detector aperture + linear motion) at the ALT direction. At the Nyquist frequency, it has a relatively high value, 12.28%, as we have not included all of the effects in ICS. This MTF_{NF} value might be higher than typical high resolution earth observation satellites [Alici K., 2019]. In laboratory measurements of satellite systems MTF targets with bar patterns may be utilized [EMVA, 2010; ISO, 2017]. Bar targets provide square wave patterns with given period. Such a square wave can be represented as a Fourier series of sinusoids. The effect of system MTF can be computed by multiplying each sinusoid coefficient with the MTF value at the specific sinusoid spatial frequency and adding the degraded series components. Dividing degraded square wave modulation to input square wave modulation yields the CTF

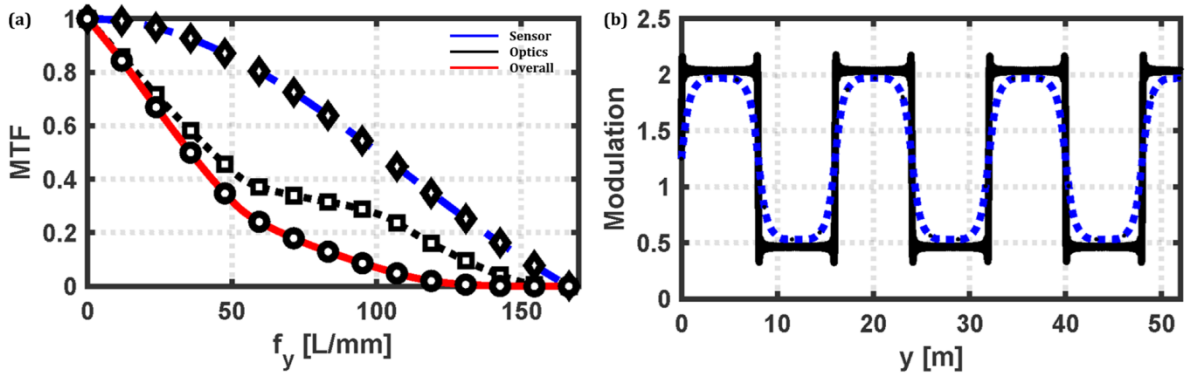

Figure 3: (a) Modulation Transfer Functions (MTF) at ALT Direction: Image Sensor MTF, Diffraction MTF, Overall System MTF, (b) Fourier series representation of input square wave modulation with ground period equal to 16 m (black-solid line), system MTF degraded square wave (blue-dashed line).

value at this specific square wave period point [Feltz J., 1990]. For example Figure 3(b) we show Fourier series representation of input square wave modulation with ground period equal to 16 m (black-solid line), and corresponding system MTF degraded square wave (blue-dashed line). In laboratory measurement utilizing bar target we obtain CTF values and corresponding MTF values could be computed as shown here. In Table 1, we list corresponding values of CTF and system MTF for our system in ALT direction.

There are a number of differences between direct image chain simulation analyses, and optoelectronic laboratory experiments [EMVA, 2010]. These may include utilization of a number of color filters in MTF measurements in laboratories for characterization and specification experiments of imaging sensors. Full scale study of differences in laboratory experiments and in orbit characterization can be studied by using our methods that are partially presented in this paper.

Table 1: Contrast Transfer Function (CTF) values for the given spatial period of bar target patterns obtained by using our satellite overall system MTF at ALT.

Period (LPW) [m]	**Spatial Freq. at Object Plane [LP/m]**	**Spatial Freq. (f_y) at Focal Plane [L/mm]**	**Overall System MTF at f_y**	**CTF at f_y**
80.0000	0.0125	2.0833	0.9738	0.8456
40.0000	0.0250	4.1667	0.9482	0.8248
20.0000	0.0500	8.3333	0.8929	0.7951
10.0000	0.1000	16.6667	0.7747	0.7457
5.0000	0.2000	33.3333	0.5325	0.5500
2.5000	0.4000	66.6667	0.2018	0.2180
2.0000	0.5000	83.3333	0.1290	0.1393
1.6667	0.6000	100.0000	0.0702	0.0759
1.4286	0.7000	116.6667	0.0243	0.0262
1.2500	0.8000	133.3333	0.0048	0.0051
1.1111	0.9000	150.0000	0.0002	0.0002
1.0000	1.0000	166.6667	0.0000	0.0000
0.6667	1.5000	250.0000	0.0000	0.0000
0.5000	2.0000	333.3333	0.0000	0.0000

Hyperbolic Wedge Resolution Analysis

SGT images that incorporate a number of well controlled resolution and MTF target patterns allows us to quantitatively study correlations between different image processing and image

quality analysis methods. We can mimic radiometric and spatial (MTF) in flight tests of spaceborne satellites, and characterization and specification laboratory tests of the cameras/image sensors, in the simulation domain. By this way, we can obtain contribution and significance of each image degrading effect (read noise, misalignment based aberrations, TDI mismatch, platform jitter, etc.) on the final image quality.

One of the standard image quality target patterns is the hyperbolic zone plates also known as hyperbolic wedge patterns (Figure 4(a)). We particularly pay attention to such patterns that are created by using the hyperbola function ($y = A_n/x$) with specifically defined A_n values for $n = 1, 2, 3, 4, 5$. The generated hyperbola shown in Figure 4(a), includes five hyperbolic black stripes with starting line width (LW) of 1.25 m in the *y-direction* (ALT). In Figure 4(b), we show the irradiance image at the focal plane (FP). Figure 4(c), resulting simulation estimate for the spaceborne AnkaraSat-3 satellite image is shown. As we look into the hyperbolic wedge pattern from left to right, at some point we cannot detect or identify individual lines anymore. That specific point, typically declared by image analysts, defines the spatial resolution of the satellite image subjectively. In this study, we aim to set a method for quantitative detection criteria by computationally scanning the image and monitoring average contrast values.

In the next subsection, we provide and compare MTF and resolution analyses results. In our future studies, we are aiming to include vertical and diagonal hyperbolic wedge patterns in order to compute vertical and diagonal spatial resolution values of the satellite system.

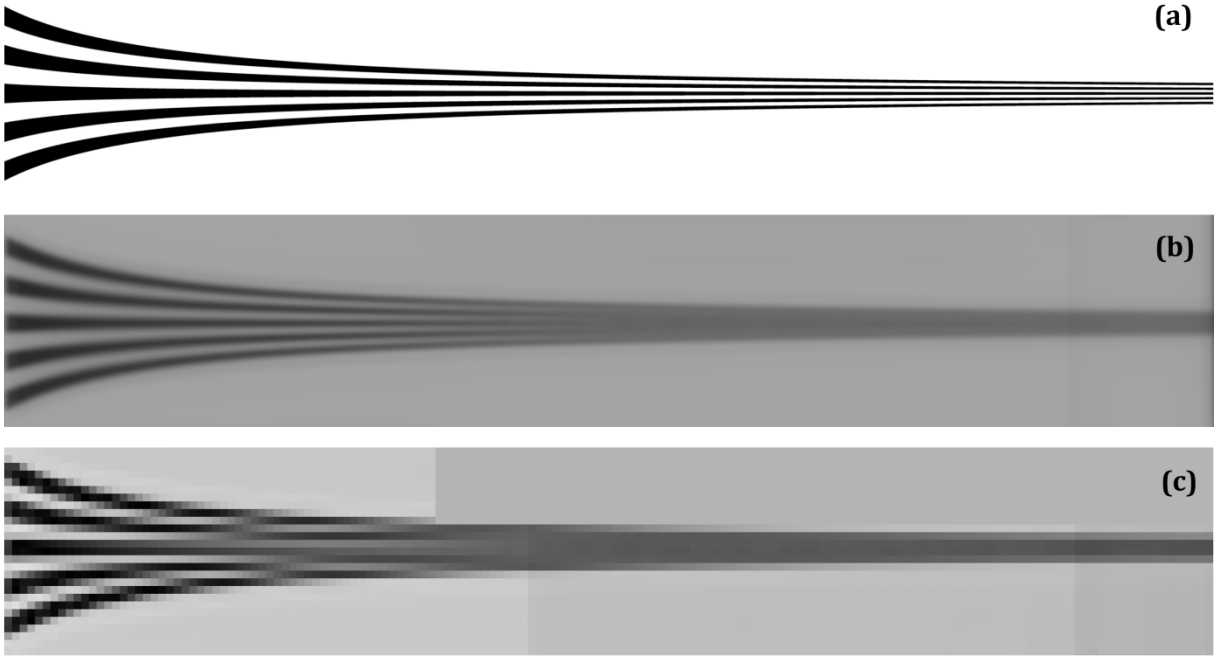

Figure 4: Hyperbolic wedge section of SGT. (a) Ground Truth with Line Pair Width (LPW) equal to 2.5 m in vertical y-direction. (b) Irradiance Image at the focal plane (FP). (c) Overall image degraded by optics and image sensor effects including diffraction, pixel aperture, and linear motion.

Comparison of MTF and Resolution Analyses Results

Modulation of a signal can be viewed best by considering addition of a constant and sinusoid signals. In that case modulation is equal to contrast in optical terminology and reduced by the system under interest specified by MTF value at that specific spatial frequency. Here, we apply the Rayleigh criterion [Fiete R., 2010; Holst G, 2011; Schott J., 2007] for spatial resolution and assume the two point sources or sinusoidal patterns are resolvable, when they are separated a distance apart known as the Airy radius. The corresponding contrast at this separation is about 15% and we apply this value to identify the minimum resolvable

spatial resolution at the hyperbolic wedge pattern. The point at which the contrast value reaches 15% is identified by simple linear search algorithm.

The spatial resolution derived from the ICS estimate of the hyperbolic wedge pattern through contrast scanning algorithm is 52.5 cm. This value corresponds to the ALT spatial frequency of $f_y = 156.6\ L/mm$. Pixel pitch ($dpix_y$) and detector aperture width at the ALT direction (y-direction) were equal to $dpix_y = 5.88\mu m$. This value corresponds to $GSD_y = 49\ cm$ at the ALT direction at 549 km altitude. As our diffraction limited optical system f-number is, $f\# = 9.72$, our system airy disk diameter (d_{airy}) is less than 4.88 times the pixel pitch: $d_{airy} < 4.88 dpix_y$ even at 1 μm sun light wavelength. Thereby, our system is detector limited system and GSD_y should correspond to spatial resolution. However, there is 6.7% discrepancy between the hyperbolic wedge spatial resolution and GSD_y results. This discrepancy depends on the SGT resolution (3.5cm) induced uncertainty, which is kept at minimum level with the current computer power limitations. We can conclude from these results that the spatial resolution automatically derived from hyper wedge satellite image estimations and GSD calculations are in good agreement. On the other hand, further investigations are necessary in the presence of optical aberrations with higher resolution SGTs that would allow $NIIRS = 9$ level real world architectures. In Table 1, we provide correspondence between the system MTF and corresponding CTF values. At very low transfer values, CTF and MTF get almost the same value and for spatial resolution detection, their difference does not have any significant effect. The spatial resolution value obtained from hyper wedge analysis (52.5 cm) is at about the point where MTF and CTF values get down to zero (highlighted in Table 1). Here we presented a candidate quantitative method for direct identification of spatial resolution, by using hyper wedge target patterns, image chain simulations and modulation analyses. We are planning to study effects of optical degradations (smaller aperture optics and/or various aberrations) on spatial resolution with higher resolution SGT input images. Moreover, by using our methods we are also planning to study effects of various subpixel geometries utilized in image sensor architectures [Alici K., 2021; Bayer B., 1976; Catrysse P., 2002; Cox J., 1981; Friedenberg A., 1997; Idema M., 2001; Kavaldjiev D., 1998].

CONCLUSIONS

To sum up, we provided a candidate quantitate method for direct identification of spatial resolution and corresponding modulation transfer function (MTF) value. We presented results of image chain simulations (ICS), spatial resolution computations, contrast transfer function (CTF), and MTF analyses, obtained by using a multi pattern synthetic ground truth (SGT) image.

ACKNOWLEDGEMENTS

The author (KBA) has been supported by the Turkish Academy of Sciences (TUBA), in the framework of the Young Scientist Award Program (TUBA-GEBIP/2020). The research study presented in this paper was the views of authors and does not reflect on the official policy of the TUBITAK, Ministry of Industry and Technology, or the Turkish government.

References

Ali M., Eltohamy F., Salama G. (2016) "Estimation of NIIRS, for high resolution satellite images, using the simplified GIQE", Int. J. Innovative Res. Comput. Commun. Eng, Vol. 4, pp. 8403-8408, 2016.

Alici K. (2019) "Image Chain Simulation for Earth Observation Satellites", IEEE Journal of Selected Topics in Applied Earth Observations and Remote Sensing, Vol. 12, pp. 4014-4023, 2019.

Alici K. (2020) "EO ve SAR Uydulari Için Karsilastirmali Görüntü Kalitesi Analizi", 8. Ulusal Havacilik ve Uzay Konferansi (UHUK-2020), 2020.

Alici K. (2021) "MTF Analysis of Metamaterial Based Imaging Sensors for Spaceborne EO/IR Remote Sensing Systems", 15th International Congress on Artificial Materials for Novel Wave Phenomena - Metamaterials 2021, 2021.

Alici K., Buyuk H., Yilmaz A., Ozdemir C., Karci O. et. al (2017) "Periodic aperture imaging", Optical Engineering, Vol. 56, 2017.

Alici K., Karci O., Yilmaz A., Ozdemir C., Oktem F. et. al (2017) "OTF analysis of a spaceborne CMOS imaging sensor", 2017 8th International Conference on Recent Advances in Space Technologies (RAST), pp. 133-138, 2017.

Alici K., Selimoglu Ö. (2018) "Yer Gözlem Uydulari Için Genel Görüntü Kalitesi Denklemi", VII. Ulusal Havacilik ve Uzay Konferansi (UHUK-2018), 2018.

Babusiaux C. (2005) "The Gaia instrument and basic image simulator", The Three-Dimensional Universe with Gaia, Vol. 576, 2005.

Barnard K., Boreman G. (1991) "Modulation transfer function of hexagonal staring focal plane arrays", Optical Engineering, Vol. 30, pp. 1915-1919, 1991.

Bayer B. (1976) "Color imaging array", United States Patent 3,971,065, 1976.

Berk A., Bernstein L., Robertson D. (1987) "MODTRAN: A moderate resolution model for LOWTRAN", SPECTRAL SCIENCES INC BURLINGTON MA, 1987.

Blahut R. (2004) "Theory of remote image formation", Cambridge University Press, 2004.

Bonier A. (1999) "The simulation of APEX data: the SENSOR approach", Imaging Spectrometry, Vol. 5, 1999.

Boreman G. (2001) "Modulation transfer function in optical and electro-optical systems", SPIE press Bellingham, WA, Vol. 4, 2001.

Brigham E. (1988) "The fast Fourier transform and its applications", Prentice-Hall, Inc., 1988.

Börner A., Wiest L., Keller P., Reulke R., Richter R. et. al (2001) "SENSOR: a tool for the simulation of hyperspectral remote sensing systems", ISPRS Journal of Photogrammetry and Remote Sensing, Vol. 55, pp. 299-312, 2001.

Catrysse P., Wandell B. (2002) "Optical efficiency of image sensor pixels", JOSA A, Vol. 19, pp. 1610-1620, 2002.

Chen T. (2003) "Digital camera system simulator and applications", Stanford University, 2003.

Coppo P., Chiarantini L., Alparone L. (2013) "End-to-End Image Simulator for Optical Imaging Systems: Equations and Simulation Examples.", Advances in Optical Technologies, 2013.

Cota S., Florio C., Duvall D., Leon M. (2009) "The use of the general image quality equation in the design and evaluation of imaging systems", Remote Sensing System Engineering II, Vol. 7458, 2009.

Cota S., Lomheim T., Florio C., Harbold J., Muto B. et. al (2011) "PICASSO: An end-to-end image simulation tool for space and airborne imaging systems II. Extension to the thermal infrared: Equations and methods", Imaging Spectrometry XVI, Vol. 8158, 2011.

Cox J. (1981) "Evaluation of peak location algorithms with subpixel accuracy for mosaic focal planes", Processing of Images and Data from Optical Sensors, Vol. 292, pp. 288-299, 1981.

Cox J. (1989) "Advantages of hexagonal detectors and variable focus for point-source sensors", Optical Engineering, Vol. 28, 1989.

EMVA (2010) "EMVA Standard 1288", European Machine Vision Association, 2010.

Elson J., Rahn J., Bennett J. (1983) "Relationship of the total integrated scattering from multilayer-coated optics to angle of incidence, polarization, correlation length, and roughness cross-correlation properties", Applied Optics, Vol. 22, pp. 3207-3219, 1983.

Estribeau M., Magnan P. (2004) "Fast MTF measurement of CMOS imagers using ISO 12333 slanted-edge methodology", Detectors and Associated Signal Processing, Vol. 5251, pp. 243-252, 2004.

Estribeau M., Magnan P. (2005) "CMOS pixels crosstalk mapping and its influence on measurements accuracy in space applications", Sensors, Systems, and Next-Generation Satellites IX, Vol. 5978, 2005.

Estribeau M., Magnan P. (2005) "Pixel crosstalk and correlation with modulation transfer function of CMOS image sensor", Sensors and Camera Systems for Scientific and Industrial Applications VI, Vol. 5677, pp. 98-108, 2005.

Farrell J., Xiao F., Catrysse P., Wandell B. (2003) "A simulation tool for evaluating digital camera image quality", Image Quality and System Performance, Vol. 5294, pp. 124-131, 2003.

Feltz J. (1990) "Development of the modulation transfer function and contrast transfer function for discrete systems, particularly charge-coupled devices [also Comment 35 (7), 2105-2106 (July 1996)] ", Optical Engineering, Vol. 29, pp. 893-904, 1990.

Fiete R. (2010) "Modeling the imaging chain of digital cameras", SPIE press Bellingham, 2010.

Filbee D., Kirk A., Stroud C., Hutchings G., Ward T. et. al (2002) "Modeling of high-fidelity synthetic imagery for defence applications", Targets and Backgrounds VIII: Characterization and Representation, Vol. 4718, pp. 12-22, 2002.

Fried D. (1966) "Limiting resolution looking down through the atmosphere", JOSA, Vol. 56, pp. 1380-1384, 1966.

Fried D. (1966) "Optical resolution through a randomly inhomogeneous medium for very long and very short exposures", JOSA, Vol. 56, pp. 1372-1379, 1966.

Friedenberg A. (1997) "Microscan in infrared staring systems", Optical Engineering, Vol. 36, pp. 1745-1749, 1997.

Gaskill J. (1978) "Linear systems, Fourier transforms, and optics", Wiley New York, Vol. 576, 1978.

Gilmore M., Moorhead I., Oxford D., Liddicoat T., Filbee D. et. al (1999) "CAMEO-SIM: a broadband scene generation system that is fit for purpose", Targets and Backgrounds: Characterization and Representation V, Vol. 3699, pp. 217-228, 1999.

Goodman J. (2015) "Statistical optics", John Wiley & Sons, 2015.

Goody R., Yung Y. (1995) "Atmospheric radiation: theoretical basis", Oxford university press, 1995.

Green R. (1998) "Summaries of the Seventh JPL Airborne Earth Science Workshop January 12-16, 1998", 1998.

Harrington L. (2015) "General image quality equation: GIQE version 5", Nat. Geospatial-Intell. Agency, Fort Belvoir, VA, USA, Tech. Rep, 2015.

Harvey J., Choi N., Schroeder S., Duparre A. (2012) "Total integrated scatter from surfaces with arbitrary roughness, correlation widths, and incident angles", Optical Engineering, Vol. 51, 2012.

Holst G., Lomheim T. (2011) "CMOS/CCD sensors and camera systems. Washington", United States: SPIE Press, 2011.

Hook R., Stoehr F. (2008) "WFC3 support in Tiny Tim", STScI Instrument Science Report WFC3-2008-014 (available from www. stsci. edu/hst), 2008.

Hufnagel R., Stanley N. (1964) "Modulation transfer function associated with image transmission through turbulent media", JOSA, Vol. 54, pp. 52-61, 1964.

Hulst H., van de Hulst H. (1981) "Light scattering by small particles", Courier Corporation, 1981.

ISO (2017) "International Standard ISO 12233:2017", ISO, 2017.

Idema M. (2001) "Sub-pixel techniques to improve spatial resolution", , 2001.

Iftekharuddin K., Karim M. (1993) "Acquisition by staring focal-plane arrays: pixel geometry effects", Optical Engineering, Vol. 32, pp. 2649-2656, 1993.

Irvine J. (1997) "National imagery interpretability rating scales (NIIRS): overview and methodology", Airborne Reconnaissance XXI, Vol. 3128, pp. 93-103, 1997.

Kavaldjiev D., Ninkov Z. (1998) "Subpixel sensitivity map for a charge-coupled device", Optical engineering, Vol. 37, pp. 948-954, 1998.

Kovalevsky J. (2013) "Modern astrometry", Springer Science & Business Media, 2013.

Krist J., Hook R., Stoehr F. (2011) "20 years of Hubble Space Telescope optical modeling using Tiny Tim", Optical Modeling and Performance Predictions V, Vol. 8127, 2011.

Leachtenauer J. (1997) "General image-quality equation: GIQE", Applied optics, Vol. 36, pp. 8322-8328, 1997.

Lei F., Tiziani H. (1993) "Atmospheric influence on image quality of airborne photographs", Optical Engineering, Vol. 32, pp. 2271-2280, 1993.

Li J., Liu J., Hao Z. (2006) "Geometrical modulation transfer function of different active pixel of CMOS APS", 2nd International Symposium on Advanced Optical Manufacturing and Testing Technologies: Optical Test and Measurement Technology and Equipment, Vol. 6150, 2006.

Li T., Feng H., Xu Z. (2011) "A new analytical edge spread function fitting model for modulation transfer function measurement", Chinese Optics Letters, Vol. 9, 2011.

Limbach M., Groff T., Kasdin N., Brandt T., Mede K. et. al (2014) "ERIS: the exoplanet high-resolution image simulator for CHARIS", Ground-based and Airborne Instrumentation for Astronomy V, Vol. 9147, 2014.

Majumdar A., Ricklin J. (2010) "Free-space laser communications: principles and advances", Springer Science & Business Media, Vol. 2, 2010.

Mathworks (2021) "www.mathworks.com", 2021.

Mendis S., Kemeny S., Gee R., Pain B., Kim Q. et. al (1994) "Progress in CMOS active pixel image sensors", Charge-Coupled Devices and Solid State Optical Sensors IV, Vol. 2172, pp. 19-29, 1994.

Mersereau R. (1987) "Hexagonal pixels, arrays, and sampling", Infrared Systems and Components, Vol. 750, pp. 57-61, 1987.

Moorhead I., Gilmore M., Houlbrook A., Oxford D., Filbee D. et. al (2001) "CAMEO-SIM: a physics-based broadband scene simulation tool for assessment of camouflage, concealment, and deception methodologies", Optical Engineering, Vol. 40, pp. 1896-1905, 2001.

O'Neill E. (1956) "Transfer function for an annular aperture", JOSA, Vol. 46, pp. 285-288, 1956.

Packard C., Curran A., Saur N., Rynes P. (2015) "Simulation-based sensor modeling and at-range target detection characterization with MuSES", Infrared Imaging Systems: Design, Analysis, Modeling, and Testing XXVI, Vol. 9452, 2015.

Rojas F. (2002) "Modulation transfer function analysis of the moderate resolution imaging spectroradiometer (MODIS) on the TERRA satellite", The University of Arizona, 2002.

Ryan R., Baldridge B., Schowengerdt R., Choi T., Helder D. et. al (2003) "IKONOS spatial resolution and image interpretability characterization", Remote sensing of environment, Vol. 88, pp. 37-52, 2003.

Sadot D., Kopeika N. (1994) "Effects of absorption on image quality through a particulate medium", Applied optics, Vol. 33, pp. 7107-7111, 1994.

Salvaggio C. (1994) "Multispectral synthetic scene generation using atmospheric propagation and thermodynamic models", State University of New York College of Environmental Science and Forestry, 1994.

Schott J. (2007) "Remote sensing: the image chain approach", Oxford University Press on Demand, 2007.

Schott J., Gerace A., Brown S., Gartley M., Montanaro M. et. al (2012) "Simulation of image performance characteristics of the Landsat data continuity mission (LDCM) thermal infrared sensor (TIRS)", Remote Sensing, Vol. 4, pp. 2477-2491, 2012.

Segl K., Guanter L., Gascon F., Kuester T., Rogass C. et. al (2015) "S2eteS: An end-to-end modeling tool for the simulation of Sentinel-2 image products", IEEE Transactions on Geoscience and Remote Sensing, Vol. 53, pp. 5560-5571, 2015.

Segl K., Kaster T., Rogap C., Kaufmann H., Sang B. et. al (2012) "EeteS: An end-to-end image simulation tool applied to THE EnMAP hyperspectral mission", Proc. 2012 IEEE Int. Geosci. Remote Sens. Symp.(IGARSS), pp. 5025-5028, 2012.

Spectral Sciences Inc. (2021) "www.modtran.spectral.com", 2021.

Taylor E. (2000) "Evaluation of multidisciplinary design optimization techniques as applied to spacecraft design", 2000 IEEE Aerospace Conference. Proceedings (Cat. No. 00TH8484), Vol. 1, pp. 371-384, 2000.

Thinkmate (2021) "www.thinkmate.com", 2021.

Turner M. (2000) "An interactive simulation environment for end-to-end digital imaging system design and fidelity analysis", The College of William and Mary, 2000.

Tzannes A., Mooney J. (1995) "Measurement of the modulation transfer function of infrared cameras", Optical Engineering, Vol. 34, pp. 1808-1817, 1995.

Welford W. (2017) "Aberrations of optical systems", Routledge, 2017.

Yadid-Pecht O. (2000) "Geometrical modulation transfer function for different pixel active area shapes", Optical Engineering, Vol. 39, pp. 859-865, 2000.